Moment-Method Analysis of Volume Dielectric Scatterers. Four Independent Entire-Domain Solutions: Is Entire-Domain Philosophy a Luxury or Necessity in the Method of Moments?

Branko D. Popović and Branislav M. Notaroš

Department of Electrical Engineering, University of Belgrade, P.O. Box 816, 11001 Belgrade, Yugoslavia. E-mail: ebdp.@ubbg.eft.bg.ac.yu

Received January 29, 1996; revised May 27, 1996.

ABSTRACT

Four independent methods are presented for entire-domain (large-domain) moment-method analysis of lossy, inhomogeneous dielectric scatterers. They share two basic steps in solving volume integral equations: (1) the approximation of the scatterer geometry by large trilinear hexahedrons; and (2) the approximation of the unknown vector function in the hexahedrons by three-dimensional polynomials. The results are compared among themselves and with those obtained by subdomain (the only existing) methods, demonstrating great superiority of the entire-domain approach in solving three-dimensional scattering and interaction problems. © 1996 John Wiley & Sons, Inc.

INTRODUCTION

The first rudiments of what is now known as the method of moments (MOM) can be traced to the early 1950s [1]. However, only the well-known 1968 monograph by R. F. Harrington [2] made it clear that the MOM was a general, extremely powerful tool for the solution of electromagnetic problems. For two decades, almost no other method was used for numerical solution of such problems. Only relatively recently have alternatives to the MOM been proposed. Probably, the most popular of these is the finite-difference time-domain (FD-TD) sequential technique for direct solution of Maxwell's differential equations [3]. It has a number of advantages, but also two principal disadvantages when compared with the MOM: it requires supercomputers, and the solution has not been so far restricted to the source region only. On the other hand, the MOM technique has been used mostly in its subdomain version; for example, as far as the authors are informed, in all studies dealing with volume dielectric scatterers the subdomain approach was used. This greatly limits the applicability of the MOM, due to the very large number of unknowns and the resulting frequently prohibitive computer time needed for the solution.

An alternative which, in the authors' opinion, can extend greatly the applicability of the method of moments is the use of the so-called entire-domain technique. Since the term "entire domain" may be misleading, it is useful at this point to define it precisely.

The literal meaning of the term "entire domain" may suggest that a body of interest must be considered as a single volume element and that the current (field) distribution inside this element should be approximated by a single functional series (e.g., by power series of sufficiently high order). Evidently, such a strict approach is possible only rarely (e.g., in the case of a dielectric

International Journal of Microwave and Millimeter-Wave Computer-Aided Engineering, Vol. 6, No. 6, 454–473 (1996)

CCC 1050-1827/96/060454-20

parallelepiped of any electrical size). Normally, the shape and the internal structure of the body considered dictate that it be approximated instead by a number of volume elements (e.g., it is virtually impossible to analyze a human body in the external field as a single volume element). Thus, the entire-domain approach (in its wider sense) implies that a body be approximated by a small number of as large as possible volume elements. The approximation of current (field) inside individual elements remains in the form of single functional series. Briefly, while the size of the volume elements in the subdomain approach is restricted by low order of approximating functional series, the size of the volume elements in the entire-domain approach is limited only by the structure geometry or its internal composition. Although, evidently, the term "large-domain approach" would be much more appropriate, "entire domain" (in the wider sense) seems to be accepted universally.

Quite surprisingly, in spite of its obvious advantages, the entire-domain MOM approach has been used relatively rarely for the analysis of electromagnetic systems. Notable examples of the application of the entire-domain approach in the last 20 years are extremely powerful tools for the analysis of wire antennas and scatterers [4] and metallic antennas and scatterers [5], far superior to subdomain methods. However, the advantage of the entire-domain MOM philosophy is particularly pronounced in the analysis of inhomogeneous, possibly lossy, dielectric scatterers [6]. In ref. 6, the volume integral equation for induced currents has been solved by point matching, approximating the scatterer by arbitrarily large right parallelepipeds with entire-domain three-dimensional power basis functions. Although much more powerful than any subdomain method, the approximation by parallelepipeds appeared to be its relatively weak point; for example, it is not simple to approximate properly a conical or spherical scatterer in that way.

Recently, significantly more flexible volume elements for geometrical modeling, so-called "trilinear hexahedrons," have been proposed [7]. This is a body with straight edges and curved sides, completely defined by its eight vertices. Using this volume element, which can be of any size and of quite diverse shape, in this article four entire-domain moment methods are proposed for the analysis of dielectric scatterers, possibly lossy, of arbitrary shape and inhomogeneity. The four methods solve either the volume EFIE or the volume two-potential equation. These equations are formulated in two forms. In one, the unknown is the total (conduction and polarization) current density vector and, in the other, the unknown is the equivalent electric displacement vector. For the approximation of the current density, entire-domain three-dimensional power basis functions in generally nonorthogonal local coordinates are used. For the approximation of the equivalent electric displacement vector, specific combinations of such power functions, which automatically satisfy the boundary condition for the normal component of the electric displacement vector at sides of adjacent hexahedrons, are used as basis functions instead. Finally, point matching is used for the solution of the two EFIEs, and the Galerkin method for the solution of the two-potential equations. In the latter case, the divergence theorem is used to transform the equations into a form that does not require numerical differentiation.

Computer programs have been completed based on all the four methods. Being numerically completely different, the methods can be considered independent. It was therefore possible not only to cross-check and cross-validate the four methods, but also to arrive at some general conclusions about them and to validate the entire general approach by comparing the results with those available in the literature.

As mentioned, all previous investigators using the MOM for the analysis of dielectric scatterers adhered to the subdomain philosophy. Although agreement of the results obtained by the present method with the available results was found to be excellent, the superiority of the present entire-domain method was found to be quite impressive. For example, it was possible to perform the entire-domain analysis of inhomogeneous lossy scatterers of medium (resonant) electrical size on standard personal computers, and in a relatively short time (on the order of few minutes at the most); with the subdomain approach, such problems require large computers and much longer computing time.

APPROXIMATION OF VOLUME CURRENT DISTRIBUTION IN TRILINEAR HEXAHEDRONS

The first step in the analysis of dielectric scatterers is to describe mathematically the geometry of the scatterer; i.e., to construct the (approximate)

geometrical model of the scatterer. This should be done with particular care, because it has a pronounced influence on the whole solution process.

In solutions based on the determination of the volume induced currents (or field), the scatterer volume has to be modeled by the appropriate volume geometrical elements. It is convenient to use the elements of the same type for the approximation of the entire dielectric body. In all existing methods for the analysis of dielectric scatterers, electrically small elements (cubes, tetrahedrons, or right parallelepipeds) are used for that purpose, with low-order functions for the approximation of the current (or field) inside them.

Following ref. 7, we shall use the trilinear hexahedron, given in Figure 1, as the basic element of the geometrical model of a dielectric scatterer of arbitrary shape and internal structure. A trilinear hexahedron is the geometrical body defined by the following parametric equation in the local nonorthogonal rectilinear u–v–w coordinate system:

$$\begin{aligned}\mathbf{r}(u,v,w) &= \frac{1}{\Delta u\,\Delta v\,\Delta w}[-(u-u_2)(v-v_2)(w-w_2)\mathbf{r}_{111} \\ &\quad +(u-u_2)(v-v_2)(w-w_1)\mathbf{r}_{112} \\ &\quad +(u-u_2)(v-v_1)(w-w_2)\mathbf{r}_{121} \\ &\quad -(u-u_2)(v-v_1)(w-w_1)\mathbf{r}_{122} \\ &\quad +(u-u_1)(v-v_2)(w-w_2)\mathbf{r}_{211} \\ &\quad -(u-u_1)(v-v_2)(w-w_1)\mathbf{r}_{212} \\ &\quad -(u-u_1)(v-v_1)(w-w_2)\mathbf{r}_{221} \\ &\quad +(u-u_1)(v-v_1)(w-w_1)\mathbf{r}_{222}] \\ \Delta u = u_2 - u_1, &\quad \Delta v = v_2 - v_1, \quad \Delta w = w_2 - w_1 \end{aligned} \tag{1}$$

In this equation, $\mathbf{r}(u,v,w)$ is the position vector of an arbitrary point of the trilinear hexahedron (defined by coordinates u, v, and w); r_{ijk} ($i = 1,2$, $j = 1,2$, $k = 1,2$) are the position vectors of the eight hexahedron vertices; and u_1, u_2, v_1, v_2, w_1, and w_2 are the starting and end coordinates of the hexahedron sides. We see that the trilinear hexahedron is determined uniquely by its eight vertices, which can be positioned in space arbitrarily. The edges of the trilinear hexahedron are straight, while its sides, in general, are curved.

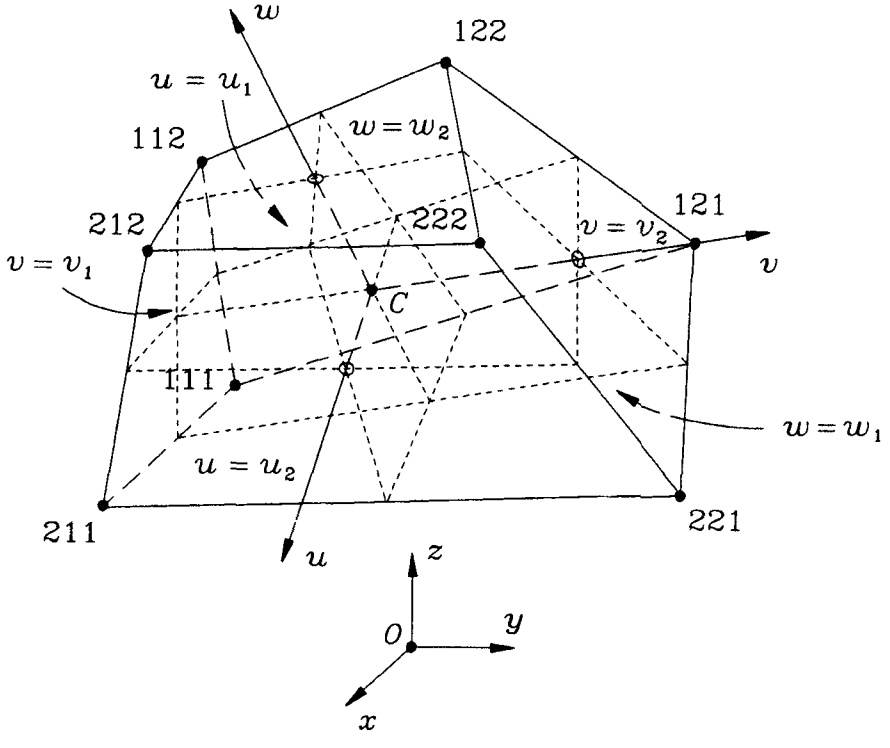

Figure 1. A trilinear hexahedron.

After elementary transformations eq. (1) can be written as:

$$\mathbf{r}(u,v,w) = \mathbf{r}_c + \mathbf{r}_u u + \mathbf{r}_v v + \mathbf{r}_w w + \mathbf{r}_{uv} uv + \mathbf{r}_{uw} uw + \mathbf{r}_{vw} vw + \mathbf{r}_{uvw} uvw, \quad u_1 \le u \le u_2, \quad v_1 \le v \le v_2, \quad w_1 \le w \le w_2 \tag{2}$$

where constant vectors $\mathbf{r}_c$, $\mathbf{r}_u$, $\mathbf{r}_v$, $\mathbf{r}_w$, $\mathbf{r}_{uv}$, $\mathbf{r}_{uw}$, $\mathbf{r}_{vw}$, and $\mathbf{r}_{uvw}$ can be determined easily.

The degrees of the three-dimensional polynomials we shall use for the approximation of the volume current distribution can be arbitrary. Therefore, the hexahedrons in the geometrical model can, in principle, be of any electrical size allowed by the geometry and the electrical properties of the body. (Of course, the electrical size of a body is subject to the limitations of the computer used for the analysis.)

The total (polarization plus conduction) current-density vector, $\mathbf{J}$, at an arbitrary point of the hexahedron (from Fig. 1) can be represented as a sum of its u-, v-, and w-components:

$$\mathbf{J}(u,v,w) = \mathbf{J}_u(u,v,w) + \mathbf{J}_v(u,v,w) + \mathbf{J}_w(u,v,w) = J_u(u,v,w)\mathbf{i}_u(u,v,w) + J_v(u,v,w) \times \mathbf{i}_v(u,v,w) + J_w(u,v,w)\mathbf{i}_w(u,v,w), \quad u_1 \le u \le u_2, \quad v_1 \le v \le v_2, \quad w_1 \le w \le w_2 \tag{3}$$

The unit vectors, $\mathbf{i}_u$, $\mathbf{i}_v$, and $\mathbf{i}_w$, which in general case are not mutually perpendicular, are obtained as:

$$\mathbf{i}_u = \frac{1}{e_u}\frac{\partial \mathbf{r}}{\partial u}, \qquad \mathbf{i}_v = \frac{1}{e_v}\frac{\partial \mathbf{r}}{\partial v}, \qquad \mathbf{i}_w = \frac{1}{e_w}\frac{\partial \mathbf{r}}{\partial w} \tag{4}$$

where e_u, e_v, and e_w are the Lamé coefficients, $e_u = |\partial \mathbf{r}/\partial u|$, $e_v = |\partial \mathbf{r}/\partial v|$, and $e_w = |\partial \mathbf{r}/\partial w|$. Note that the u-, v-, and w-coordinates are, in general, not the length coordinates.

To express the unknown functions, J_u, J_v, and J_w, in the form suitable for the further steps of the method, consider a differentially small prism at a point (u,v,w), with edges parallel to the unit vectors $\mathbf{i}_u$, $\mathbf{i}_v$, and $\mathbf{i}_w$, and of edge lengths $\mathrm{d}l_u = e_u\,\mathrm{d}u$, $\mathrm{d}l_v = e_v\,\mathrm{d}v$, and $\mathrm{d}l_w = e_w\,\mathrm{d}w$, as shown in Figure 2. The current through the prism side denoted by u can be obtained as:

$$\mathrm{d}I_u = \mathbf{J}_u \cdot \mathrm{d}\mathbf{S}_{vw} = J_u\,\mathrm{d}S_{vw}\mathbf{i}_u \cdot \mathbf{n}_{vw} = J_u(\mathrm{d}l_v\,\mathrm{d}l_w \sin\alpha_{vw})\sin\alpha_{(v,w)u} = J_u e_v e_w \sin\alpha_{vw} \sin\alpha_{(v,w)u}\,\mathrm{d}v\,\mathrm{d}w \tag{5}$$

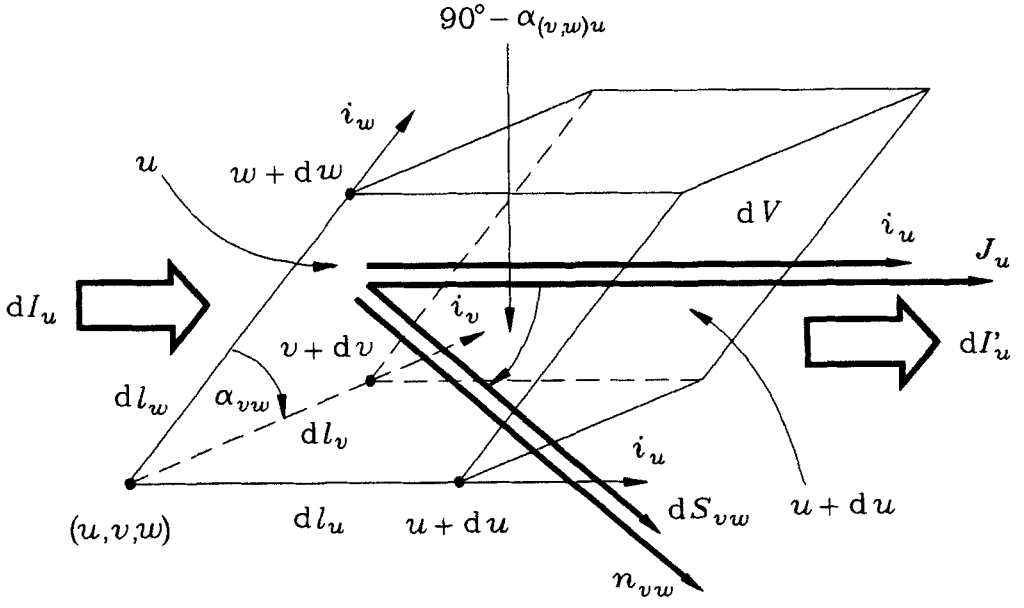

Figure 2. Infinitely small prism with edges tangent to local coordinate lines and quantities necessary for the approximation of the current-density vector in the u-v-w coordinate system.

where α_{vw} and $\alpha_{(v,w)u}$ are the angles between v and w coordinate lines (i.e., between the vectors $\mathbf{i}_v$ and $\mathbf{i}_w$) and between the u coordinate line and v–w coordinate surface, respectively, at point (u,v,w). On the basis of eq. (5), the current-density J_u can be expressed as:

$$J_u = \frac{1}{e_v e_w \sin\alpha_{vw} \sin\alpha_{(v,w)u}} \frac{\mathrm{d}I_u}{\mathrm{d}v\,\mathrm{d}w} \tag{6}$$

Analogous expressions can be derived for the components J_v and J_w of the current-density vector.

INTEGRAL EQUATIONS FOR VOLUME CURRENT DISTRIBUTION

The Lorentz potentials due to the volume current distribution $\mathbf{J}_u$ (and corresponding volume and surface charge distributions) in the arbitrary, nth element (trilinear hexahedron) of the geometrical model of a dielectric scatterer can be expressed as:

$$\mathbf{E}_n^{(u)} = -j\omega\mu_0 \int_{u_1}^{u_2}\int_{v_1}^{v_2}\int_{w_1}^{w_2} \left[\frac{\mathrm{d}I_u}{\mathrm{d}v\,\mathrm{d}w}\frac{\partial \mathbf{r}}{\partial u} + \frac{1}{\beta_0^2}\frac{\partial}{\partial u}\left(\frac{\mathrm{d}I_u}{\mathrm{d}v\,\mathrm{d}w}\right)\mathrm{grad}\right] g(R)\,\mathrm{d}u\,\mathrm{d}v\,\mathrm{d}w + \frac{j}{\omega\varepsilon_0}\sum_{l=1}^{2}(-1)^l \int_{v_1}^{v_2}\int_{w_1}^{w_2} \frac{\mathrm{d}I_u}{\mathrm{d}v\,\mathrm{d}w}\bigg|_{u=u_l} \mathrm{grad}\, g(R_l)\,\mathrm{d}v\,\mathrm{d}w \tag{9}$$

$$\mathbf{A}_n^{(u)} = \mu_0 \int_{u_1}^{u_2}\int_{v_1}^{v_2}\int_{w_1}^{w_2} \mathbf{J}_u\,\mathrm{d}V g(R) \tag{7a}$$

$$\Phi_n^{(u)} = \frac{j}{\omega\varepsilon_0}\left[\int_{u_1}^{u_2}\int_{v_1}^{v_2}\int_{w_1}^{w_2} \mathrm{div}\,\mathbf{J}_u\,\mathrm{d}V g(R) + \sum_{l=1}^{2}(-1)^{l-1} \times \int_{v_1}^{v_2}\int_{w_1}^{w_2} (\mathbf{J}_u \cdot \mathrm{d}\mathbf{S}_{vw})|_{u=u_l} g(R_l)\right] \tag{7b}$$

In these equations, $\mathrm{d}V$ is the volume of the differentially small prism from Figure 2, and $\mathrm{d}\mathbf{S}_{vw}$ is the vector surface element of the trilinear hexahedron side defined by the equation $u = u_l$ ($l = 1$ or 2). This element represents the side of the small prism, positioned at the point (u_l, v, w).

Finally, $g(R)$ is the free-space Green's function:

$$g(R) = \frac{e^{-j\beta_0 R}}{4\pi R}, \qquad \beta_0 = \omega\sqrt{\varepsilon_0\mu_0} = 2\pi/\lambda_0, \qquad R = |\mathbf{r}_f - \mathbf{r}(u,v,w)| \tag{8}$$

[$\mathbf{r}_f$ is the position vector of the field (potential) point and $\mathbf{r}(u,v,w)$ is given in eq. (2)].

The corresponding electric-field vector is $\mathbf{E}_n^{(u)} = -j\omega\mathbf{A}_n^{(u)} - \mathrm{grad}\,\Phi_n^{(u)}$. The gradient operator operates on the field-point coordinates. It can therefore be introduced under the integrals in the expression for the scalar potential, $\Phi_n^{(u)}$, in eq. (7b) and be made to operate on Green's function alone. Finally, by using eqs. (3), (4), and (6), the expressions for the volume, $\mathrm{d}V$, and the surface, $\mathrm{d}\mathbf{S}_{vw}$ (which can easily be obtained on the basis of Fig. 2), as well as the expression for $\mathrm{div}\,\mathbf{J}_u$, which can be derived starting from the general integral definition of the divergence applied to the prism in Figure 2, the following expression is obtained for calculating $\mathbf{E}_n^{(u)}$:

Note that, in this expression, the Lamé coefficients, as well as the angles α_{vw} and $\alpha_{(v,w)u}$, are not present. This is the principal reason for adopting the initial representation of function J_u as given in eq. (6). The resultant secondary field, $\mathbf{E}$, due to three local components of the current-density vector, $\mathbf{J}_u$, $\mathbf{J}_v$, and $\mathbf{J}_w$, in all (N_{el}) trilinear hexahedrons of the geometrical model, is:

$$\mathbf{E} = \mathbf{E}(\mathbf{J}) = \sum_{n=1}^{N_{\mathrm{el}}} \left[\mathbf{E}_n^{(u)} + \mathbf{E}_n^{(v)} + \mathbf{E}_n^{(w)}\right] \tag{10}$$

This field plus the incident (impressed) field, $\mathbf{E}_i$, result in the total field in dielectric, $\mathbf{E}_{\mathrm{tot}}$, which is connected with the current density, $\mathbf{J}$, by means of the generalized local Ohm's law,

$$\mathbf{J} = \sigma_e \mathbf{E}_{\mathrm{tot}}, \qquad \sigma_e = \sigma + j\omega(\varepsilon - \varepsilon_0) \tag{11}$$

where ε, σ, and σ_e are permittivity, conductivity, and equivalent complex conductivity of the dielectric, respectively, at the field point. Thus, we obtain the equation:

$$\frac{\mathbf{J}}{\sigma_e} - \mathbf{E}(\mathbf{J}) = \mathbf{E}_i \tag{12}$$

which represents the electric-field integral equation (EFIE) for an arbitrary inhomogeneous dielectric scatterer. Finally, note that by analytical differentiation of grad g in eq. (9) we have:

$$\text{grad } g(R) = -(1 + j\beta_0 R)\frac{e^{-j\beta_0 R}}{4\pi R^3}[\mathbf{r}_f - \mathbf{r}(u,v,w)] \tag{13}$$

If, however, the resultant potentials, $\mathbf{A}(\mathbf{J})$ and $\Phi(\mathbf{J})$, are first expressed by summation of the partial potentials in eqs. (7) analogous to that in eq. (10), and then the relation $\mathbf{E} = -j\omega\mathbf{A} - \text{grad } \Phi$ is utilized, the local Ohm's law results in:

$$\frac{\mathbf{J}}{\sigma_e} + j\omega\mathbf{A}(\mathbf{J}) + \text{grad}[\Phi(\mathbf{J})] = \mathbf{E}_i \tag{14}$$

This equation represents the two-potential integral equation (TPIE).

The integral kernels of the TPIE, eq. (14), contain the singularity of the lowest possible order, i.e., of the form $1/R$, and is therefore very convenient from the numerical point of view. On the other hand, it is necessary to perform numerical differentiation in evaluating grad Φ. We shall later see that, with the solution methods that imply additional integration of eq. (14), this numerical differentiation can be avoided. The EFIE in eq. (12), however, has integral kernels containing the factor $\mathbf{R}/R^3$ [see eq. (13)]. This makes the corresponding numerical integration more difficult than in the case of the TPIE.

ENTIRE-DOMAIN POLYNOMIAL APPROXIMATIONS OF VOLUME CURRENT DISTRIBUTION

Approximation of Total Current – Density Vector

Let the function J_u in an arbitrary trilinear hexahedron in the geometrical model of a scatterer be represented as in eq. (6). We approximate the unknown function $dI_u/(dv\,dw)$ by the entire-domain, three-dimensional power series (polynomial) in local coordinates:

$$\frac{dI_u}{dv\,dw} = \sum_{i=0}^{N_u}\sum_{j=0}^{N_v}\sum_{k=0}^{N_w} a_{uijk}u^i v^j w^k, \qquad \left.\begin{matrix} u_1 \le u \le u_2 \\ v_1 \le v \le v_2 \\ w_1 \le w \le w_2 \end{matrix}\right\} \tag{15}$$

where N_u, N_v, and N_w are the degrees of the polynomial that can be adopted arbitrarily, and a_{uijk}, a_{vijk}, and a_{wijk} are unknown complex coefficients to be determined. The expansions analogous to those in eqs. (6) and (15) are adopted for the components J_v and J_w. We adopt power basis functions because, on the one hand, they are quite simple and allow for rapid evaluation. On the other hand, they are very flexible, so that with a relatively low degree polynomial it is possible to approximate accurately quite diverse functions.

Few comments about the boundary condition for the normal component of the total current–density vector, $\mathbf{J}$, may be useful at this point. Namely, if $\mathbf{J}$ is treated as unknown in the adopted integral equation, the total (polarization and free) surface charge density, ρ_s, at the boundary surface between any two adjacent trilinear hexahedrons is evaluated for each hexahedron separately, as $\rho_s = -(j/\omega)\mathbf{n} \cdot \mathbf{J}$ [see eq. (7b)]. Therefore, the trilinear hexahedrons are totally independent entities, so that in a geometrical model they can be positioned and interconnected arbitrarily. On the other hand, because the condition $\rho_s = 0$ at the surfaces shared by hexahedrons having the same electrical properties is satisfied only numerically, theoretically nonexistent surface charges may result from an inaccurate numerical solution of a problem. For example, for a model composed of trilinear hexahedrons in the form of small cubes of the same dielectric, and zero-degree polynomials ($N_u = N_v = N_w = 0$) used for the approximation of current inside them, physically nonexistent surface charges must appear at boundary surfaces— otherwise, current density in all the small cubes would be the same. These surface charges may cancel one another to a significant degree, and thus may have negligible influence on the far field. Most frequently, how-

ever, their existence significantly impairs the accuracy of the field inside the small cubes and in their immediate vicinity.

Approximation of Equivalent Electric Displacement Vector

Alternatively, it is possible to substitute **J** as the unknown in volume integral equations by the equivalent electric displacement vector, defined by:

$$\mathbf{D} = \varepsilon_e \mathbf{E}_{\text{tot}} = \mathbf{J}/(j\omega K),$$
$$\varepsilon_e = \varepsilon - j\sigma/\omega = \varepsilon_{er}\varepsilon_0, \qquad K = \frac{\varepsilon_e - \varepsilon_0}{\varepsilon_e} \tag{16}$$

where ε_e and K are the equivalent complex permittivity and electric contrast of the dielectric, respectively. The normal component of **D** is continuous at boundary surfaces between different dielectrics. Let us consider only the u-component of **D**, $\mathbf{D}_u = D_u \mathbf{i}_u$, in a trilinear hexahedron. The function D_u we initially represent in the same manner as J_u [see eq. (6)]:

$$D_u = \frac{1}{e_v e_w \sin\alpha_{vw} \sin\alpha_{(v,w)u}} \frac{\mathrm{d}\Psi_u}{\mathrm{d}v\,\mathrm{d}w} \tag{17}$$

$\mathrm{d}\Psi_u$ being the inward flux of vector $\mathbf{D}_u$ through the side of the infinitesimal prism from Figure 2 denoted by u. Next, we approximate the function $\mathrm{d}\Psi_u/(\mathrm{d}v\,\mathrm{d}w)$ by the following series:

$$\begin{aligned}\frac{\mathrm{d}\Psi_u}{\mathrm{d}v\,\mathrm{d}w} = &\sum_{j=0}^{N'_v}\sum_{k=0}^{N'_w} b_{u0jk}(1-u)v^j w^k \\ &+ \sum_{j=0}^{N''_v}\sum_{k=0}^{N''_w} b_{u1jk}(1+u)v^j w^k \\ &+ \sum_{j=0}^{N_v}\sum_{k=0}^{N_w}\Bigg[\underbrace{\sum_{i=2}^{N_u} b_{uijk}(u^i-1)}_{(2)} \\ &+ \underbrace{\sum_{i=3}^{N_u} b_{uijk}(u^i-u)}_{(2)}\Bigg]v^j w^k\end{aligned} \tag{18}$$

The starting and end local coordinates are adopted to be $u_1 = v_1 = w_1 = -1$ and $u_2 = v_2 = w_2 = 1$ in each trilinear hexahedron of the model.

The expansion defined by eqs. (17)–(18) represents three-dimensional entire-domain polynomial series with unknown complex coefficients b_{uijk}, that satisfies automatically the continuity condition for the normal component of vector **D** on the surfaces shared by adjacent trilinear hexahedrons in the geometrical model of an arbitrary dielectric scatterer. Let us make this evident. It can be shown that the continuity condition for vector $\mathbf{D}_{\text{norm}}$ on a boundary surface of two hexahedrons reduces to the condition of equality of the values of function $\mathrm{d}\Psi_u/(\mathrm{d}v\,\mathrm{d}w)$ on the two sides of that surface. The basis functions $(1-u)v^j w^k$ (for $i = 0$) and $(1+u)v^j w^k$ (for $i = 1$) in an arbitrary hexahedron serve for adjusting that condition on the side $u = -1$ and $u = 1$, respectively, while the remaining basis functions (for $i \geq 2$) serve for improving the approximation of the function D_u, as illustrated in Figure 3 for the chain of three trilinear hexahedrons. In doing this, $(N'_v + 1)(N'_w + 1)$ coefficients, b_{u0jk} (for $i = 0$), and $(N''_v + 1)(N''_w + 1)$ coefficients, b_{u1jk} (for $i = 1$), in any hexahedron are the same as the corresponding coefficients in adjacent hexahedrons; i.e., a certain number of coefficients are the same for any two adjacent hexahedrons. In this manner the number of unknown coefficients for a problem, in general, is reduced significantly. Of course, as the vector **D** in the air is not considered unknown, functions $(1 \pm u)v^j w^k$ on the boundary surface of a hexahedron and air do not have their match. Finally, the polynomial degrees N_u, N_v, and N_w in eq. (18) can be adopted for every hexahedron separately, while N'_v represents the smaller value of N_v for two adjacent hexahedrons on the corresponding shared side, and analogous explanations hold for N'_w, N''_v, and N''_w.

Obviously, the geometrical model of a dielectric scatterer has to be constructed in a way which guarantees that each boundary surface between two adjacent trilinear hexahedrons over which we want to (automatically) adjust the boundary condition for $\mathbf{D}_{\text{norm}}$ is shared entirely by both of them. This is a simple task, because every side of a trilinear hexahedron is defined uniquely by its four vertices, which can be positioned in space completely arbitrarily.

In addition to the reduction in the number of unknowns, the use of the approximation defined by eqs. (17)–(18) results in increased accuracy and stability of the results, and prevents fictitious surface charges to appear in the numerical solution on the surfaces shared by any two hexahe-

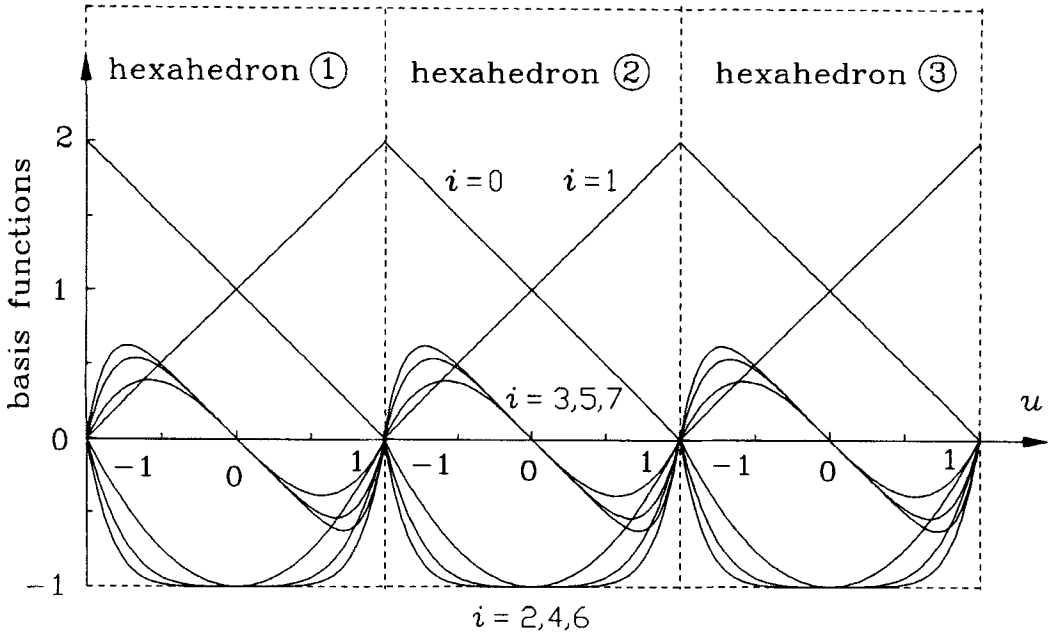

Figure 3. First eight basis functions in coordinate u defined in eq. (18), for $v = w = 1$.

drons made of the same dielectric. On the other hand, the solution with vector **D** as the unknown is mathematically much more complicated, and, in some cases, numerically less advantageous than if **J** is used instead (with the current approximation proposed earlier). This will be demonstrated by corresponding numerical examples later in this study.

TEST PROCEDURES

Point-Matching Method

The simplest test procedure (i.e., the procedure for determining the current-distribution coefficients, $[a]$ or $[b]$) is the point-matching method [2]. In our case, the position vectors of matching points are given by $\mathbf{r}(u^{(p)}, v^{(s)}, w^{(t)})$, where $\mathbf{r}(u, v, w)$ is defined in eq. (2) and p, s, and t are the corresponding indices. In the basic version of the point-matching method we shall adopt matching points to be equidistant along each local coordinate in a trilinear hexahedron:

$$u^{(p+1)} - u^{(p)} = \text{const} \tag{19}$$

with the starting and endpoints being at a distance, $e_u\,\delta u$, from the corresponding hexahedron sides, where e_u is the Lamé coefficient, and δu is given by:

$$\delta u = \eta \frac{u_2 - u_1}{N_u} \tag{20}$$

We adopt the distributions of matching points along v- and w-coordinates in an analogous manner. As a rule, the parameter η should be adopted as small as possible ($\eta \ll 1$), with the intention to incorporate the field components at points close to boundary surfaces; i.e., the field components that enter the boundary conditions, into the resulting system of linear equations. In the case of only one matching point along the u-coordinate (e.g., if $N_u = 0$), we adopt $u^{(0)} = (u_1 + u_2)/2$.

Equidistant matching points may not be the best choice. For example, if in reality there is a rapid variation of the unknown quantity between two matching points, this may not be reflected properly in the solution if no matching points are adopted in that region. Unfortunately, we rarely know the solution even vaguely. Therefore, it is of interest to solve a problem with a set of nonequidistant matching points. There is an infinite number of possibilities for such a set. With the intention to sample more accurately the field close to hexahedron sides, as the set of nonequidistant matching points we adopt their distribution according to the arguments of the Gauss–Legendre integration (quadrature) for-

mula. In that case we have:

$$u^{(p)} = u_1 + (u_2 - u_1)(x_G)_{p+1} \qquad (21)$$

where $(x_G)_{p+1}$ $(p = 0, 1, \ldots, N_u)$ are the arguments of the Gauss–Legendre formula of order $N_G = N_u + 1$; i.e., the zeros of the corresponding Legendre polynomial. Analogous expressions hold for coordinates $v^{(s)}$ and $w^{(t)}$.

In the case of approximation of vector **D** defined by eqs. (17)–(18), pairs of matching points are formed on the two sides of a boundary surface between adjacent trilinear hexahedrons, and the normal local field components at these points are added up. This is necessary because the corresponding number of coefficients [b] is the same for each pair of adjacent hexahedrons.

After some transformations it can be shown that the electric-field vector and the potentials, due to currents and charges inside the adopted model of a dielectric scatterer, needed in the point-matching solution with both forms of the polynomial current approximation as well as with both integral equations, are linear combinations of four basic types of integrals. The integrands in these integrals are three- or two-dimensional power functions multiplied by Green's function or its gradient, and the integration is performed over the volume of a trilinear hexahedron (Fig. 1) or over its side. According to the combined analytical/numerical integration procedures that have been developed for the evaluation of the basic types of integrals [7], for points inside the trilinear hexahedron or close to its surface the principal parts of the integrals are extracted and integrated analytically, while the individual numerical integrations were performed by the multiple Gauss–Legendre integration formula. This formula in conjunction with the polynomial basis functions enables very rapid recursive evaluation of multiple integrals.

Galerkin Method

If the Galerkin method [2] is adopted, however, the EFIE in eq. (12) results in the following equation:

$$\left\langle \mathbf{f}_m, \frac{\mathbf{J}}{\sigma_e} \right\rangle - \langle \mathbf{f}_m, \mathbf{E}(\mathbf{J}) \rangle = \langle \mathbf{f}_m, \mathbf{E}_i \rangle \qquad (22)$$

where $\langle \mathbf{f}_m, \mathbf{E} \rangle$ is the inner scalar product over the volume V_m of the mth trilinear hexahedron in the geometrical model of the scatterer, and $\mathbf{f}_m$ is the weighting (testing) function defined in that hexahedron. Of course, in a Galerkin method, the weighting functions are the same as the basis functions defined earlier.

On the other hand, the Galerkin method with the TPIE in eq. (14) results in an equation analogous to eq. (22), which contains the term $\langle \mathbf{f}_m, \mathrm{grad}[\Phi(\mathbf{J})] \rangle$. To avoid numerical differentiation implied in grad Φ, this term can be transformed by expanding $\mathrm{div}(\mathbf{f}_m \Phi)$ and applying the divergence theorem. By doing this we obtain:

$$\langle \mathbf{f}_m, \mathrm{grad}[\Phi(\mathbf{J})] \rangle = -\int_{V_m} \Phi(\mathbf{J}) \mathrm{div}\, \mathbf{f}_m \, dV_m + \oint_{S_m} \Phi(\mathbf{J}) \mathbf{f}_m \cdot d\mathbf{S}_m \qquad (23)$$

where $\mathbf{S}_m$ is the boundary surface of the mth trilinear hexahedron and $d\mathbf{S}_m$ is directed outward with respect to th domain V_m. After some algebraic transformations, the corresponding generalized impedances (i.e., the system-matrix elements) can be represented in the following form:

$$\begin{aligned} Z_{mn}^{(u,u)} = {} & \int_{u_{1m}}^{u_{2m}} \int_{v_{1m}}^{v_{2m}} \int_{w_{1m}}^{w_{2m}} \frac{1}{\tau_e} \left[\left(\frac{\partial \mathbf{r}}{\partial u} \times \frac{\partial \mathbf{r}}{\partial v} \right) \cdot \frac{\partial \mathbf{r}}{\partial w} \right]_m^{-1} \\ & \times \left(F \frac{\partial \mathbf{r}}{\partial u} \right)_m \left(F \frac{\partial \mathbf{r}}{\partial u} \right)_n du_m \, dv_m \, dw_m \\ & + j\omega \int_{u_{1m}}^{u_{2m}} \int_{v_{1m}}^{v_{2m}} \int_{w_{1m}}^{w_{2m}} \left(F \frac{\partial \mathbf{r}}{\partial u} \right)_m \\ & \times \mathbf{A}_n^{(u)} \, du_m \, dv_m \, dw_m \\ & - \int_{u_{1m}}^{u_{2m}} \int_{v_{1m}}^{v_{2m}} \int_{w_{1m}}^{w_{2m}} \frac{\partial F_m}{\partial u_m} \Phi_n^{(u)} \, du_m \, dv_m \, dw_m \\ & + \sum_{p=1}^{2} (-1)^p \int_{v_{1m}}^{v_{2m}} \int_{w_{1m}}^{w_{2m}} F_m |_{u = u_{pm}} \\ & \times \Phi_n^{(u)} \, dv_m \, dw_m \end{aligned} \qquad (24)$$

where $Z_{mn}^{(u,u)}$ corresponds to the u-component of the testing function **f** in the mth hexahedron and the u component of **J** or **D** in the nth one. F denotes an arbitrary term of the testing series in eq. (15)—in the case of approximation of **J**, namely of that in eq. (18)—if **D** is treated as an unknown quantity. In addition, τ_e designates σ_e, namely ε_e, in the case of approximation of **J**, namely **D**, respectively. Finally, $\mathbf{A}_n^{(u)}$ and $\Phi_n^{(u)}$ represent the potentials due to current distribution (and the corresponding charge distributions) re-

lated to the individual basis functions defined in eq. (15), i.e. eq. (18) (in the nth hexahedron). They are evaluated on the basis of eqs. (7). The corresponding integration procedures have been very briefly discussed in the previous subsection.

When using testing and basis functions given in eq. (18), aimed at automatically satisfying the continuity condition for $\mathbf{D}_{\text{norm}}$ on the surfaces shared by adjacent trilinear hexahedrons, certain impedances $Z_{mn}^{(u,u)}$, evaluated on the basis of eq. (24), are added together with the corresponding impedances which relate to the hexahedrons adjacent either to the mth or to the nth hexahedron.

Finally, by solving the resulting system of linear algebraic equations we find the N_{un} unknown complex coefficients $[a]$ or $[b]$. In this article, the Gauss elimination procedure is adopted for that purpose, with both test procedures outlined in this section. Once this has been completed, all the quantities of interest can be evaluated directly.

FOUR SPECIFIC METHODS BASED ON THE GENERAL ENTIRE-DOMAIN APPROACH FOR ANALYSIS OF DIELECTRIC SCATTERERS

On the basis of the general theory outlined in the previous sections, the following four independent entire-domain methods have been developed for the analysis of inhomogeneous dielectric scatterers:

1. The point-matching method for solving the EFIE, eq. (12), with the current density vector, **J**, as the unknown. We shall refer to this method briefly as to the PEJ method.
2. The Galerkin method for solving the TPIE, eq. (14), with the current density vector, **J**, as the unknown (the GPJ method).
3. The point-matching method for solving the EFIE, eq. (12), with the equivalent electric displacement vector, **D**, as the unknown (the PED method).
4. The Galerkin method for solving the TPIE, eq. (14), with the equivalent electric displacement vector, **D**, as the unknown (the GPD method).

As explained, the basis functions adopted for the approximation of the current-density vector are given in eq. (15), and those for the approximation of the equivalent electric displacement vector in eq. (18). In all four methods, the scatterer is approximated by trilinear hexahedrons.

Four accompanying computer programs have been completed, enabling four independent methods of numerical analysis of dielectric scatterers. Numerical results presented in the next section were obtained using these programs.

NUMERICAL RESULTS AND DISCUSSION

All numerical results obtained by the four proposed methods have been obtained on a PC-486/66 MHz (8-MB DRAM). The programs were written in Lahey F77L-EM/32 Fortran 77. For scatterers with curved surfaces, the geometrical model was always constructed so that the surface of the model approximated the scatterer surface in the best possible manner, with the condition that the volume of the model and the volume of the scatterer were the same. Symmetry was not utilized in any example.

The most critical quantity in the analysis of dielectric scatterers is certainly the total electric field inside it. If it is accurate, the scattered field will certainly be accurate. This is why in practically all examples which follow particular attention was paid to the total electric field inside the scatterer.

As the first example, consider a homogeneous lossless dielectric cube of relative permittivity $\varepsilon_r = 4$, illuminated by a plane wave of electric field strength $\mathbf{E}_i = 1 \exp(-j\beta_0 z)\mathbf{i}_x$ V/m (Fig. 4). Let the length of the cube edge be $a = \lambda_0 = 2\lambda_d$, where λ_d represents the wavelength in the dielectric. Shown in Figure 5 is the distribution of the x-component of the total electric field, $\mathbf{E}_{\text{tot}}$, inside the cube, along the x-axis, obtained by the four methods. The authors could not find any reliable results for the electric field inside a cubic dielectric scatterer.

The cube was represented exactly by a single trilinear hexahedron ($N_{e1} = 1$). In all four methods it was assumed that $N_u = N_v = N_w = 4$, which resulted in $N_{\text{un}} = 375$ unknowns. In the PEJ and PED methods, matching points were adopted according to the arguments of the Gauss-Legendre integration formula, eq. (21). Excellent agreement among the four sets of results can be observed. All the four methods required $T_{\text{sys}} \approx 55$ s for the solution of the resulting system of equations, and the field evaluation for Figure 5 and other output computations needed about 2 s. The matrix fill

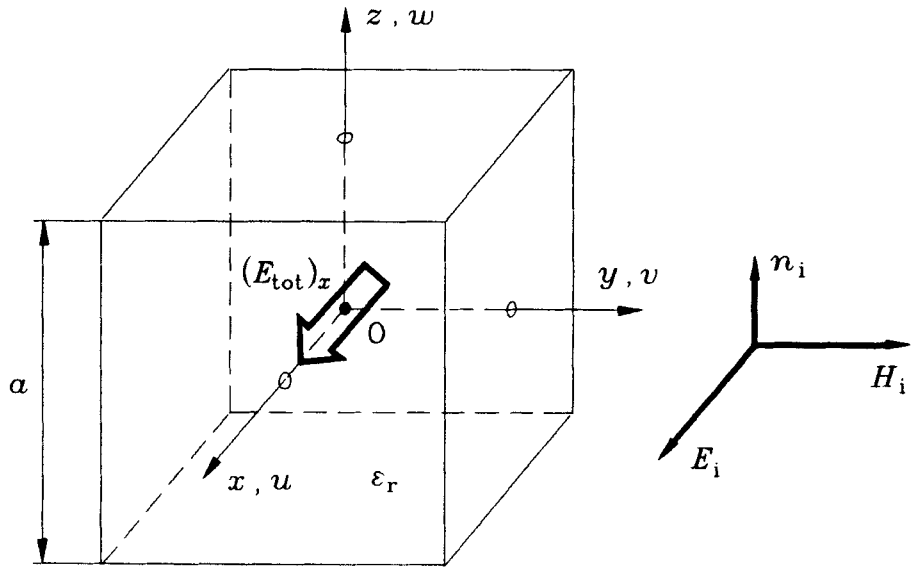

Figure 4. A homogeneous dielectric cube in an incident, linearly polarized plane wave. The origin is at the cube center.

times, including all operations preceding them, were as follows: $(T_{mat})_{PEJ} = 42.45$ s, $(T_{mat})_{GPJ} = 49.16$ s, $(T_{mat})_{PED} = 45.53$ s, and $(T_{mat})_{GPD} = 54.21$ s. As expected, the matrix fill time for the two Galerkin-based methods is somewhat longer than for the two point-matching methods, and additional time is needed in the case of more complex basis functions used for the approximation of vector **D**. Note, however, that the differences in the matrix fill times are actually surpris-

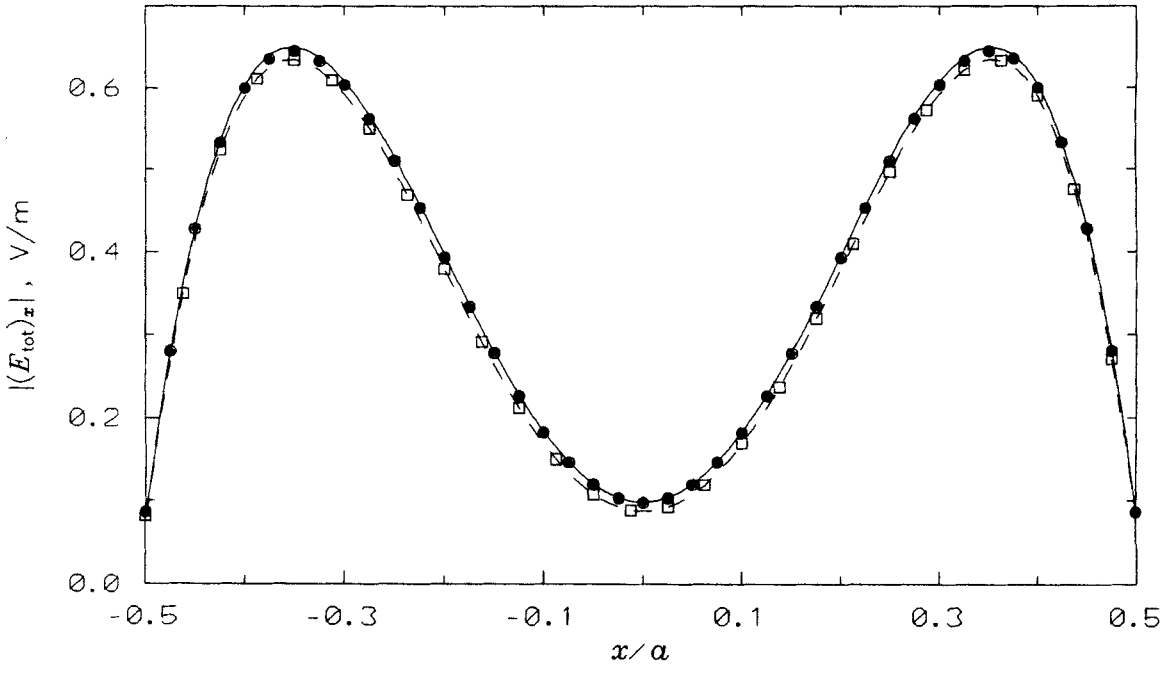

Figure 5. Distribution of magnitude of the x-component of the total electric field, $\mathbf{E}_{tot}$, inside the cube in Figure 4, for $\varepsilon_r = 4$, $a = \lambda_0 = 2\lambda_d$, and $\mathbf{E}_{i0} = 1$ V/m, along the x-axis. (□) PEJ method; (●) GPJ method; (--) PED method; — GPD method.

ingly small if one has in mind that the Galerkin method requires another (volume or surface) integration. This is due to extremely efficient integration of the Galerkin integrals in the generalized impedances in eq. (24) [7].

Contrary to the results for the inner field, a number of results can be found in the literature for the far scattered field of a dielectric cube. The next example deals with the far scattered field of a dielectric cube, Figure 4, with $\varepsilon_r = 4$ and $a = \lambda_0/5 = 2\lambda_d/5$ (electrically small cube). Shown in Figure 6 are the results for the far scattered field obtained by the GPD method in two characteristic planes, normalized with respect to the maximal value of that field. The results obtained by the other three methods are practically the same and are not shown. The adopted degrees of approximation were $N_u = N_v = N_w = 2$. The number of unknowns amounted to only $N_{\text{un}} = 81$, and the total computing time to $T_{\text{tot}} = 5.48$ s. These results are compared with those obtained by a subdomain method, 3D pulse approximations of vector **J** in 512 small cubes (1536 unknowns), and point-matching solution of the TPIE, in which grad Φ was evaluated by finite differences [8]. Figure 6 shows excellent agreement of the two sets of results, in spite of the number of unknowns in the proposed entire-domain method being almost 20 times less than in the subdomain method of ref. 8.

Illustrated in Figure 7a is the cross-section of a sphere consisting of two homogeneous lossless dielectric half-spheres of relative permittivity $\varepsilon_{r1} = 8$ and $\varepsilon_{r2} = 4$. Let the electric field vector of the incident wave be $\mathbf{E}_i = 1 \exp(-j\beta_0 z)\mathbf{i}_y$ V/m, and the sphere diameter $d = 2a = \lambda_0 = 2.343(\lambda_d)_{\text{av}}$, where $(\lambda_d)_{\text{av}} = (\lambda_{d1} + \lambda_{d2})/2$. Each half-sphere in Figure 7a is approximated by one trilinear hexahedron, as shown in Figure 7b, so that $N_{e1} = 2$. The same degrees of approximation were adopted in the four methods, $N_u = N_v = N_w = 3$, in both hexahedrons. Matching points were adopted according to the arguments of the Gauss–Legendre integration formula. In the PEJ and GPJ methods, in which the unknown is vector **J**, the total number of unknowns amounted to

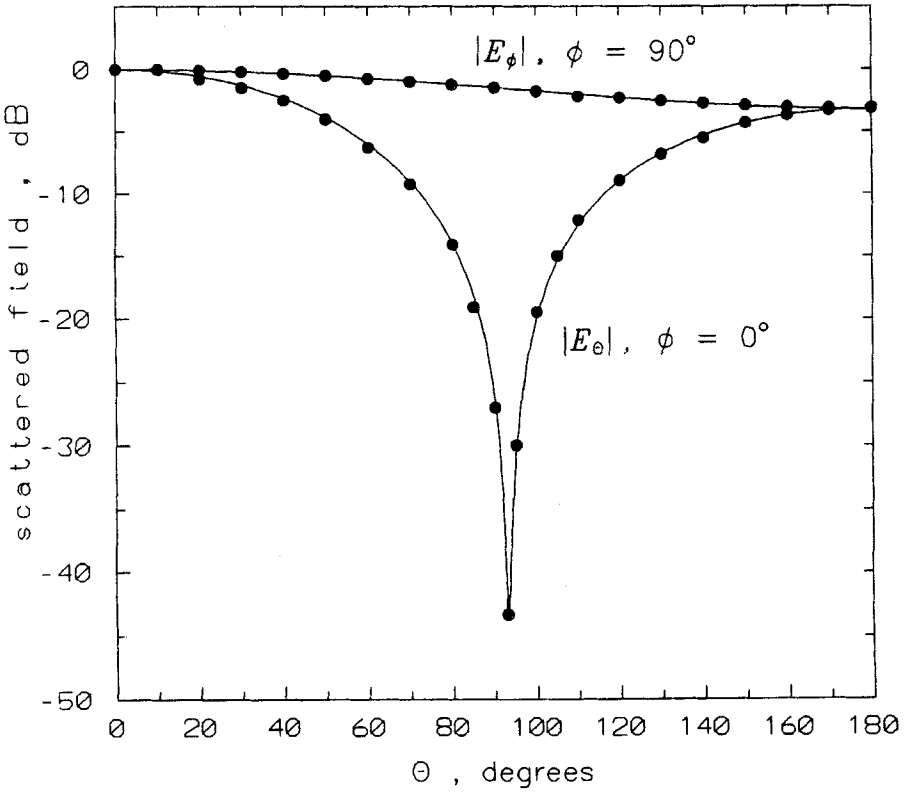

Figure 6. Normalized far scattered field, $20 \log|E/E_{\max}|$, of a homogeneous dielectric cube described in caption to Figure 5, of side length $a = \lambda_0/5 = 2\lambda_d/5$, versus θ, in planes $\phi = 0°$ and $\phi = 90°$. (—) GPD method, 81 unknowns; (●●●) method from ref. 8, 1536 unknowns.

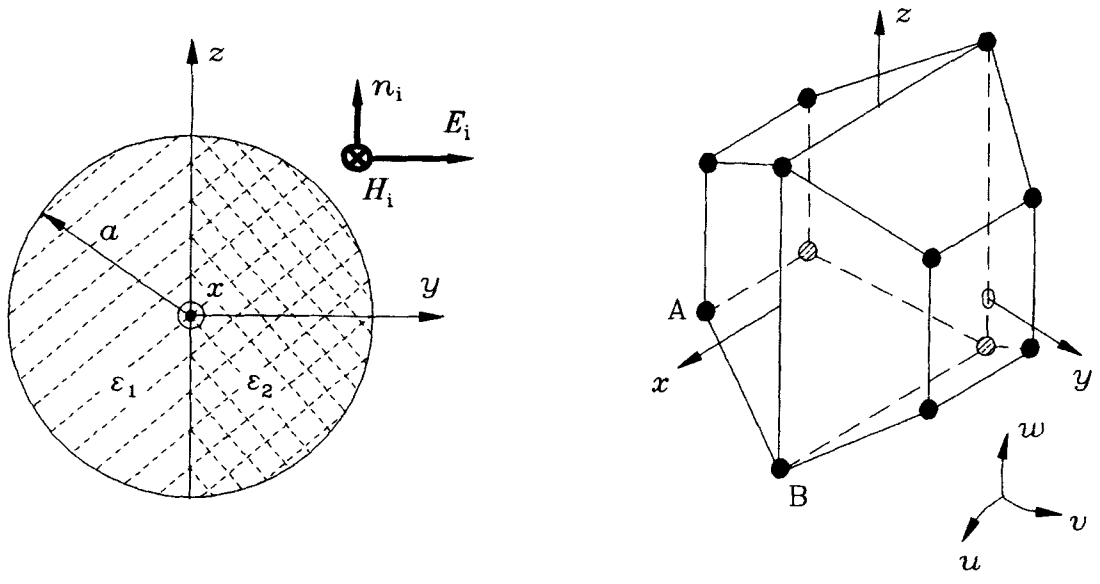

(a) (b)

Figure 7. A sphere consisting of two homogeneous hemispheres, in an incident plane wave. (a) Cross-section of the sphere. (b) Model of the sphere consisting of two trilinear hexahedrons; $\mathbf{r}_A = (0.4678a, -1.0226a, -0.4678a)$ and $\mathbf{r}_B = (0.9354a, 0.0, -0.9354a)$.

$N_{un} = 384$, while in the other two methods it amounted to $N_{un} = 368$.

Illustrated in Figure 8a is the distribution of the y-component of the total inner electric field, $|(E_{tot})_y|$, along the y-axis, obtained by the four methods, showing good agreement of the four sets of results. Note that the results obtained by the point-matching method on one side, and those obtained by the Galerkin method on the other side, are in excellent agreement, but that the two sets of results differ to some extent. It is quite likely that those obtained by the Galerkin method are more accurate, due to another integration, but the other results are also of acceptable accuracy.

Let us concentrate our attention to the field values in the vicinity of the point $y = 0$ in Figure 8a. This part of the figure is shown magnified in Figure 8b. In the PED and GPD methods, irrespective of the overall quality of the solution, the boundary condition $|(E_{tot})_y(0^-)|/|(E_{tot})_y(0^+)| = 4/8 = 0.5$ is satisfied exactly, being equivalent to the condition $D_{norm}(0^-) = D_{norm}(0^+)$ satisfied by all matching pairs of basis functions. It is seen from Figure 8b that the solutions obtained by the other two methods satisfy this boundary condition very well, despite that it was not enforced, but followed from the numerical solution. Evidently, this shows very good approximation of current and charge distribution.

As the next example, consider a rodlike scatterer of length $l = 2\lambda_0 = 4.739\lambda_d$, of square cross-section of area $\lambda_0^2/100$, made of a homogeneous lossy dielectric of complex permittivity $\varepsilon_{er} = 4 - j6$ (Fig. 9). Let the incident electric field be $\mathbf{E}_i = 1\exp(-j\beta_0 z)\mathbf{i}_x$ V/m. Figure 10 shows the distribution of the total inner electric field, $\mathbf{E}_{tot}$, along the scatterer long axis. The results given are obtained by two methods which show the largest difference, the PEJ and the GPD methods. In all cases, it was assumed that $N_{el} = 1$; i.e., the rod was considered as a single tetrahedron.

In the GPD method, it was assumed that $N_u = 8$ and $N_v = N_w = 1$. This resulted in $N_{un} = 108$ and $T_{tot} = 10.99$ s. The PEJ method was tested in the following six forms:

1. Matching points distributed according to eq. (21), $N_v = N_w = 0$ and $N_u = 8$. This resulted in $N_{un} = 27$ and $T_{tot} = 1.15$ s (PEJ1).
2. Matching points, N_v and N_w as in form 1, and $N_u = 12$. This resulted in $N_{un} = 39$ (PEJ2).
3. Matching points distributed along the scatterer axis according to eq. (19), with $N_u = 12$, $N_v = N_w = 0$ and $\eta = 0.01$ in eq. (20) (PEJ3).
4. Same as form 3, with $N_u = 8$, $N_v = N_w = 1$, and $\eta = 0.01$ (PEJ4).

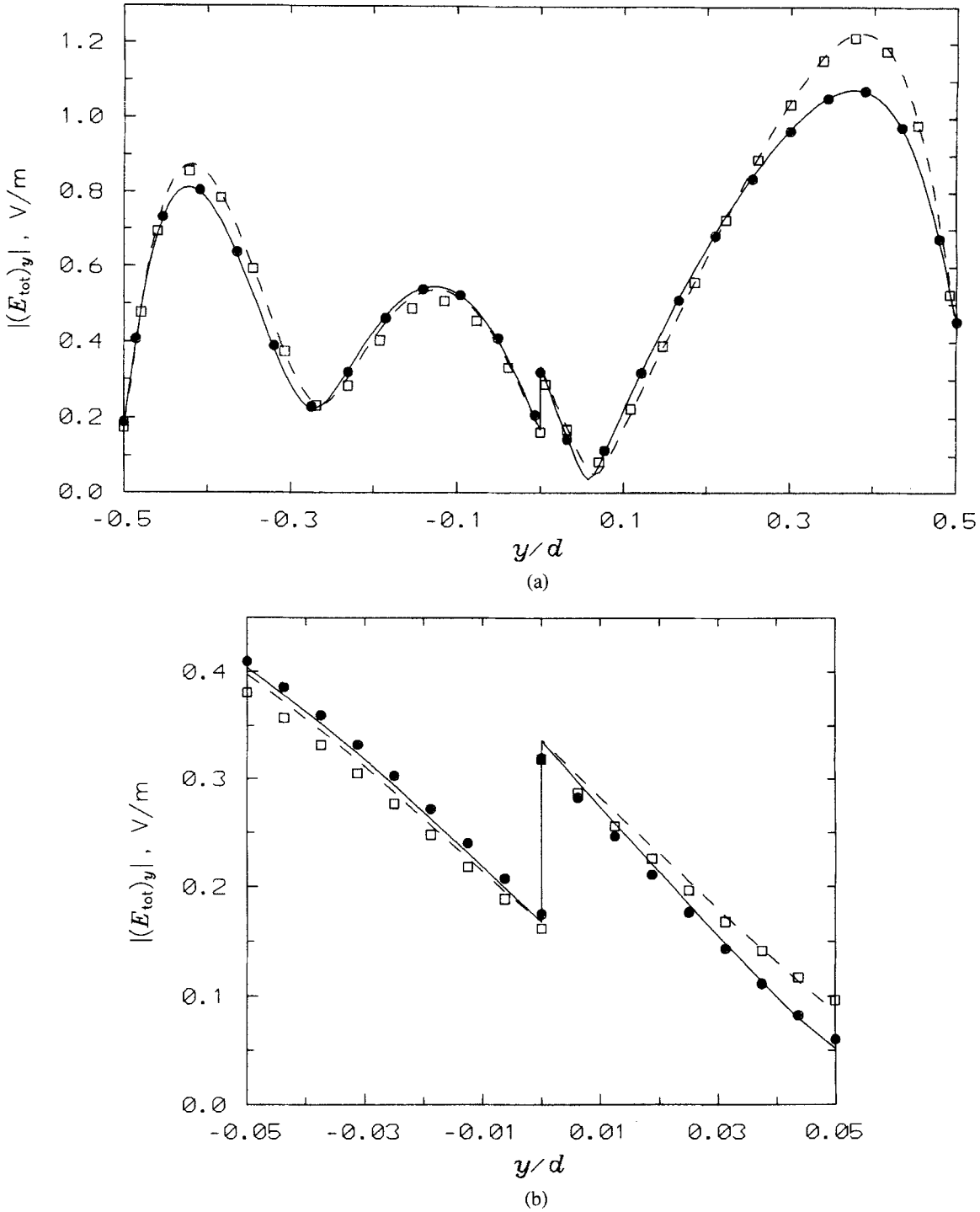

Figure 8. (a) Distribution of the total electric field inside the sphere in Figure 7, with $\varepsilon_{r1} = 8$, $\varepsilon_{r2} = 4$, $d = 2a = \lambda_0$, and $\mathbf{E}_i = 1 \exp(-j\beta_0 z)\mathbf{i}_y$ V/m, along the y-axis. (b) Detail of (a) at $y = 0$. (□) PEJ method; (●) GPJ method; (--) PED method; — GPD method.

5. Same as form 4, with $\eta = 0.001$ (PEJ5).
6. Same as form 4, with $\eta = 0.1$ (PEJ6).

Figure 10 shows good agreement between the results obtained by the GPD method and those obtained by forms (1), (3), and (6) of the PEJ method. The results obtained by form 2 of the PEJ method, however, are meaningless. This is very likely the consequence of some of the $N_u + 1 = 13$ matching points, distributed according to

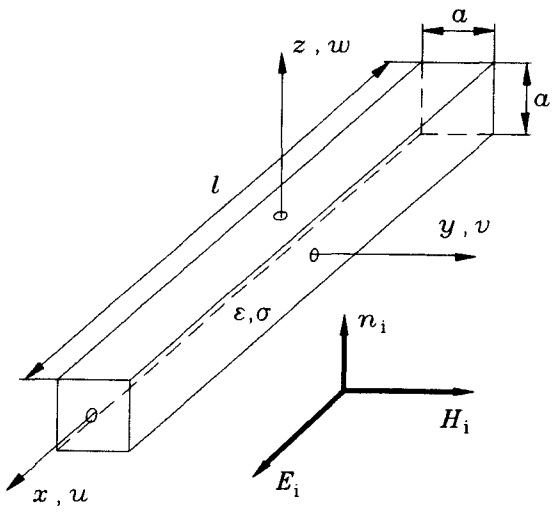

Figure 9. A rodlike homogeneous lossy dielectric scatterer of square cross-section.

eq. (21), being very close, so that the resulting system of linear equations is highly unstable. The results obtained by forms 4 and 5 of the PEJ method have relatively large discrepancies in local field values close to scatterer ends. This could probably be explained by matching points not being along the scatterer axis (as when $N_v = N_w = 0$), but being very close ($\eta = 0.01$ or 0.001) to the edges and vertices of the scatterer, where the electric field varies very rapidly. On the other hand, in form 3 of the PEJ method ($N_v = N_w = 0$) the choice of the parameter, η, in the range $0 < \eta \leq 0.1$ was found to have practically no influence on the results.

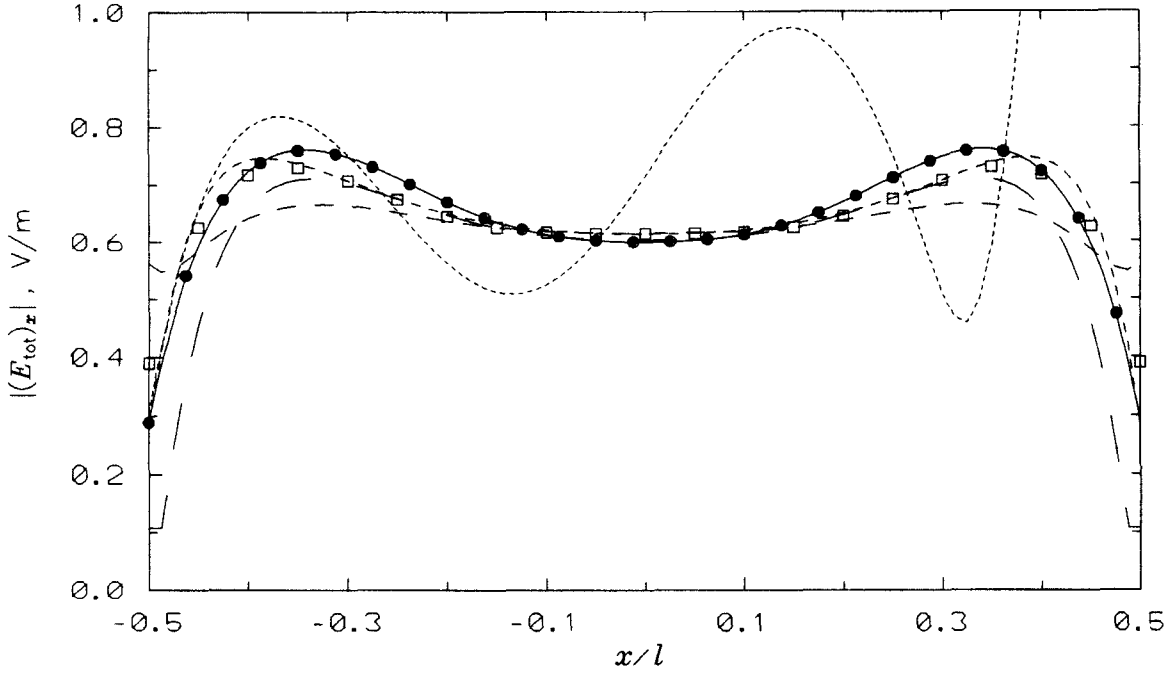

Figure 10. Distribution of the total inner electric field, $\mathbf{E}_{\text{tot}}$, along the long axis of the rodlike scatterer in Figure 9, with $l = 2\lambda_0 = 4.739\lambda_d$, $a = \lambda_0/10$, $E_{i0} = 1$ V/m, and $\varepsilon_{er} = 4 - j6$. (-----) GPD; (——) PEJ1; (··· ···) PEJ2; (● ● ●) PEJ3; (– – –) PEJ4; (——) PEJ5; (□ □ □) PEJ6.

Consequently, the distribution of matching points according to eq. (21) in the case of high orders of approximation leads to unstable results, whereas for equidistant matching points and nonzero order of approximations the results depend on parameter η. Of course, such problems are not present with the Galerkin method. Finally, this example shows a deficiency of the two methods in which the unknown is vector **D**. Namely, the minimal order of polynomial approximation of vector **D**, defined earlier, is 1, so that it was not possible to adopt $N_v = N_w = 0$ along electrically very short edges of the rod scatterer. This resulted in an unnecessarily large total number of unknowns ($N_{\text{un}} = 108$) in the application of the GPD method.

As an example of rapid convergence of the results, consider again the total field inside the scatterer from Figure 9, but with the degree N_u of the polynomial approximation along the scatterer axis as the parameter. Acceptable results were obtained with N_u as low as 4, and the results for $N_u = 6$ and those for $N_u = 8$ were practically the same. Note that the rodlike scatterer analyzed is of medium electrical length ($l = 4.739\lambda_d$). Similar convergence properties were found in all other cases considered.

Consider next a cube of edge length $a = 0.5\lambda_0$, consisting of four homogeneous parts of equivalent relative complex permittivities $\varepsilon_{er1} = 2.5 + j0$, $\varepsilon_{er2} = 5 + j0$, $\varepsilon_{er3} = 3 - j4$, and $\varepsilon_{er4} = 8 - j6$ (Fig. 11). The cube is situated in the field of an incident plane wave of electric field $\mathbf{E}_i = 1 \exp(-j\beta_0 z)\mathbf{i}_x$ V/m. Figure 12 shows the distribution of real part, imaginary part, and modulus of the x-component of the vector $\mathbf{E}_{\text{tot}}$ along the x-axis. Every homogeneous part of the cube is represented by one hexahedron ($N_{el} = 4$), and it was assumed that $N_v = N_w = 4$ in all of them. The results were obtained in four ways: (1) by the GPD method with $N_u = 1$ in all the elements ($N_{\text{un}} = 525$, $T_{\text{tot}} = 320.76$ s); (2) by the GPJ method with $N_u = 1$ ($N_{\text{un}} = 600$); (3) by the GPJ method with $N_u = 0$ ($N_{\text{un}} = 300$); and (4) by the application of a specific form of the GPD method which results in $N_{\text{un}} = 240$ and $T_{\text{tot}} = 142.92$ s. In the latter case, $N_u = 1$ was adopted, but the orders of approximation for individual components of the vector **D** in transversal directions (with respect to the direction of that component) were reduced for $\Delta N_{\text{tran}} = 1$. Thus, for example, the terms of the highest order in the expansion for the D_u-component are proportional to $(1 \pm u)v^3w^3$, whereas the expansion for the D_v-compo-

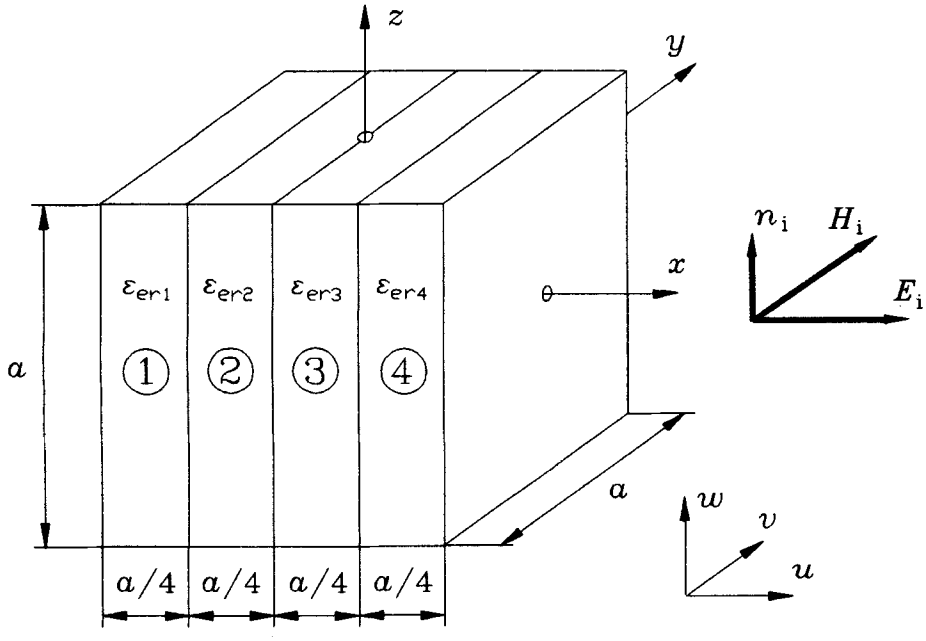

Figure 11. A dielectric cube consisting of four homogeneous parts in the field of a plane wave.

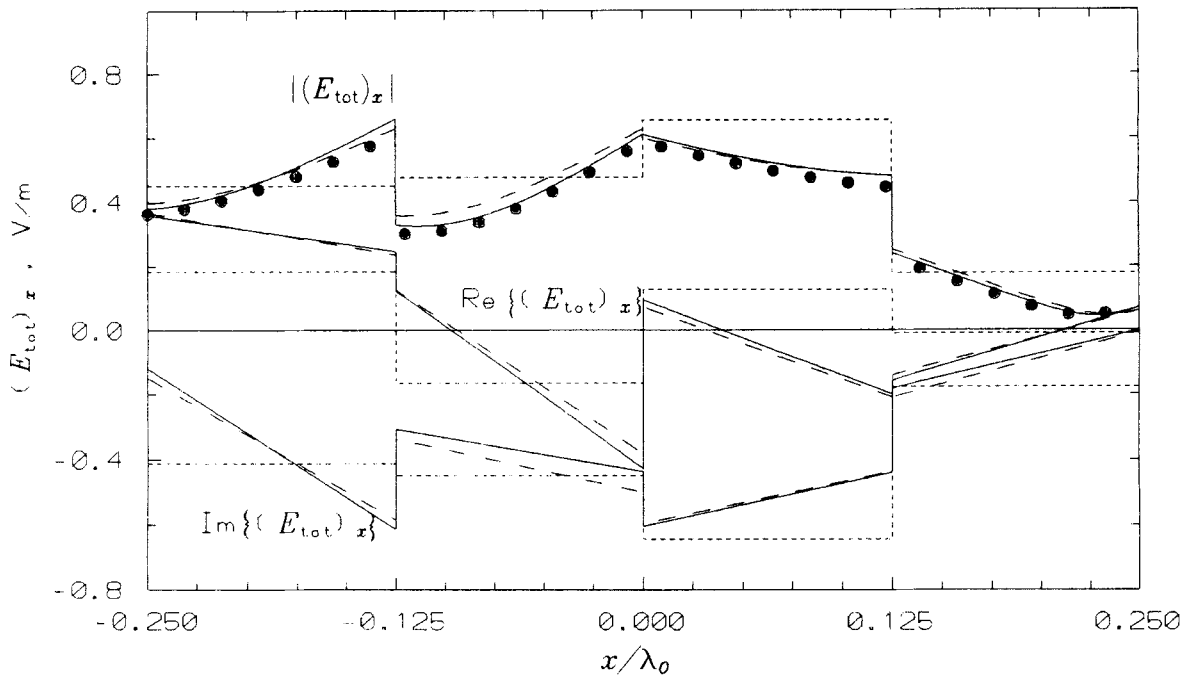

Figure 12. Distribution of the total inner electric field, $(E_{\text{tot}})_x$ along x-axis, for dielectric cube from Figure 11, with $a = 0.5\lambda_0$, $\varepsilon_{er1} = 2.5 + j0$, $\varepsilon_{er2} = 5 + j0$, $\varepsilon_{er3} = 3 - j4$, $\varepsilon_{er4} = 8 - j6$, and $\mathbf{E}_{i0} = 1$ V/m. (——) GPD method, $N_u = 1$, $N_{\text{un}} = 525$; (---) GPJ method, $N_u = 1$, $N_{\text{un}} = 600$; (··· ···) GPJ method, $N_u = 0$, $N_{\text{un}} = 300$; (●●●) GPD method ($\Delta N_{\text{tran}} = 1$), $N_u = 1$, $N_{\text{un}} = 240$.

nents contains the highest-order term of the form $u^0(v^4 - 1)w^3$ [see eq. (18)].

Figure 12 shows good agreement of the sets of the results (1), (2), and (4). Note that the number of unknowns in result (2) is greater than in result (1) for about 14% because there are no common terms in adjacent volume elements. Note also that, by adopting $\Delta N_{\text{tran}} = 1$ in result (4), the total number of unknowns is more than halved with respect to result (1), and the total computing time is reduced for more than 50%. On the other hand, result (3), obtained with piecewise constant approximation of vector **J** along the x-axis, at some points differs considerably from findings obtained with piecewise linear approximation, although qualitatively they are not so much in error.

It is of interest to check the degree of fulfillment of the boundary condition for vector $(\varepsilon_e \mathbf{E}_{\text{tot}})_{\text{norm}}$ in planes $x = -0.25a$, $x = 0$, and $x = 0.25a$ in Figure 11. The exact ratios of the complex vector intensities are $(2 + j0)$, $(0.6 - j0.2)$ and $(1.92 + j0.56)$, respectively. The corresponding numerically obtained ratios are: $(2 + j0)$, $(0.6 - j0.8)$, and $(1.92 + j0.56)$ for results (1) and (4); $(1.755 + j0.04527)$, $(0.7532 - j0.7309)$, and $(1.893 + j0.2667)$ for result (2); and $(0.6748 + j0.6616)$, $(0.6206 - j0.3795)$, and $(3.573 + j0.9220)$ for result (3). Of course, the boundary conditions in results (1) and (4), where the unknown is vector **D**, are satisfied exactly. The boundary conditions in result (2), piecewise linear approximation of vector **J**, are satisfied with fair accuracy; whereas, in result (3), piecewise constant approximation of vector **J**, the results show large errors.

As the last example, consider a thin elliptical disk of the shape shown in Figure 13 in dashed lines. Let the major and minor semiaxes of the ellipse be $a = 0.64\lambda_0$ and $b = 0.32\lambda_0$, and the disk thickness (normal to the plane of the figure) be $d = 0.08\lambda_0$. Assume that the electric field of the incident plane wave is $\mathbf{E}_i = 1 \exp[-j\beta_0(x + z\sqrt{3})/2]\mathbf{i}_y$ V/m, and that the disk is made of a lossless, but inhomogeneous, dielectric of relative permittivity:

$$\varepsilon_r(x, y, z) = 2 - \left[\left(\frac{x}{a}\right)^2 + \left(\frac{y}{b}\right)^2\right], \quad \left(\frac{x}{a}\right)^2 + \left(\frac{y}{b}\right)^2 \le 1, \quad |z| \le \frac{d}{2} \tag{25}$$

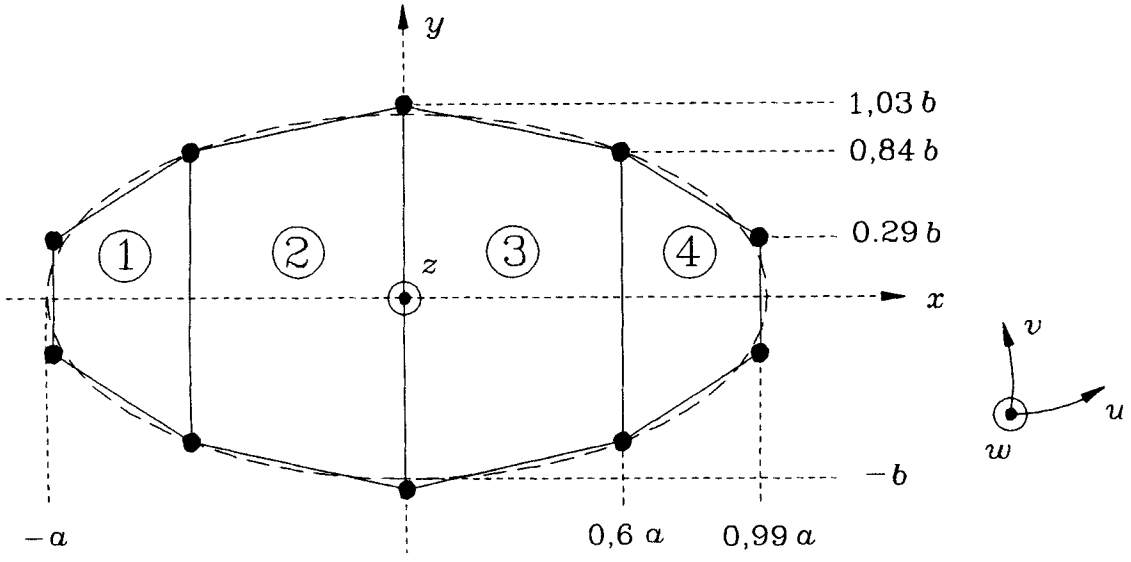

Figure 13. Top view of a thin elliptical disk (---) and its approximation (——) by trilinear hexahedrons.

The elliptical disk is modeled quite accurately with only $N_{el} = 4$ trilinear hexahedrons, as indicated in Figure 13. The PEJ method is used for the analysis, with matching points according to eq. (21). It was assumed that $N_u = 2$, $N_v = 4$, and $N_w = 0$ in all the four hexahedrons, which resulted in $N_{un} = 180$ and $T_{tot} = 21.81$ s. Note that all trilinear hexahedrons in the model contain continually inhomogeneous dielectrics. Figure 14 shows the results for the normalized bistatic cross-section, S_{bist}/λ_0^2, of the disk, in the planes $\phi = 0$ and $\phi = 180°$. These entire-domain results are compared with subdomain results from ref. 9, where the disk is approximated by a large number of small homogeneous parallelepipeds with a 3D pulse approximation of the field. The latter results were multiplied by 0.5, because Su [9] apparently presented $20\log(S_{bist}/\lambda_0^2)$ instead of the usual $10\log(S_{bist}/\lambda_0^2)$.

It is seen that, in the case of the inhomogeneous dielectric disk from Figure 13, the proposed entire-domain method enabled the approximation of the disk by only four trilinear hexahedrons containing a continuously inhomogeneous dielectric, while the subdomain approach required very fine division of the disk into a large number of small elements with approximately constant permittivity.

CONCLUSIONS

A general entire-domain MOM approach and four independent methods within this approach are proposed for the analysis of lossy dielectric scatterers of arbitrary shape and inhomogeneity. The approach consists in solving a volume integral equations using two basic steps: (1) the approximation of the scatterer geometry by large trilinear hexahedrons; and (2) the approximation of the unknown vector function in the hexahedrons by three-dimensional polynomials. The first two methods consider the total current density vector, **J**, as the unknown, approximated by simple three-dimensional power series in three generally nonorthogonal coordinates. In the other two methods, the equivalent electric displacement vector, **D**, is the unknown, approximated by specific power series which automatically satisfy boundary conditions for the normal components of vector **D** at boundary surfaces of adjacent hexahedrons. The first and the third method solve the volume EFIE by point matching, and the second and the fourth the volume two-potential equation by the Galerkin method in which numerical differentiation is removed.

In spite of the four methods being completely independent numerically, the results obtained by them, in most cases, are in excellent agreement.

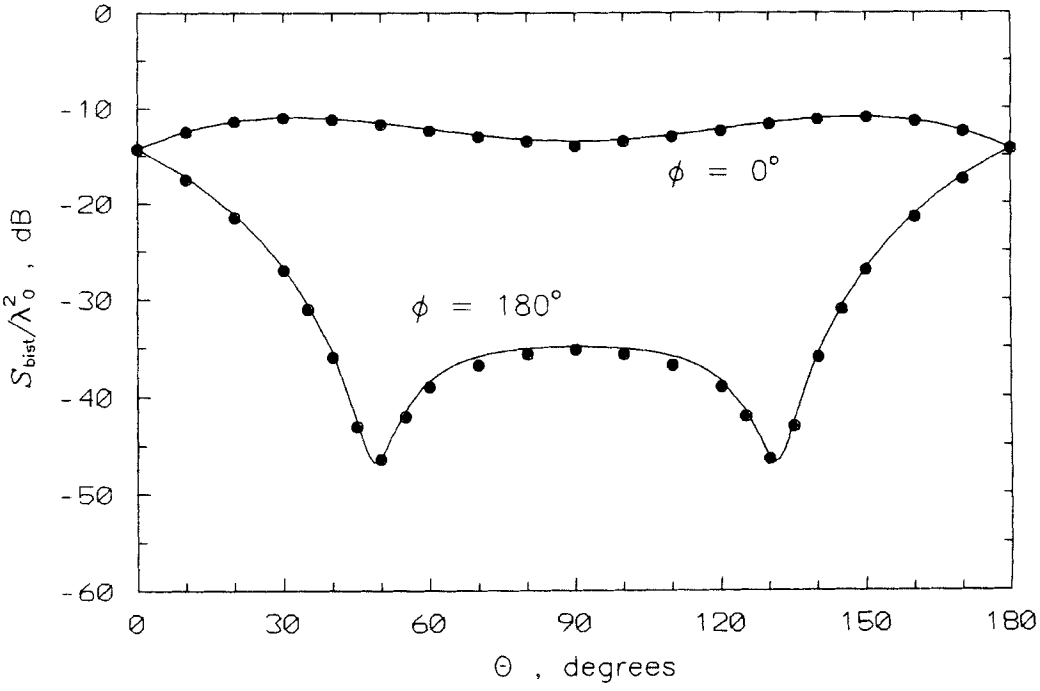

Figure 14. Normalized bistatic cross-section, $10\log(S_{\text{bist}}/\lambda_0^2)$, of the inhomogeneous disk in Figure 13, of permittivity in eq. (25), versus θ, in planes $\phi = 0°$ and $\phi = 180°$, for $\mathbf{E}_i = 1\exp[-j\beta_0(x + z\sqrt{3})/2]\mathbf{i}_y$ V/m. (——) PEJ method, $N_{e1} = 4$, $N_{\text{un}} = 180$; (●●●) ref. 9.

In addition, they are in excellent agreement with all available results of other authors (obtained by subdomain methods), in spite of requiring at least one order of magnitude fewer unknowns, with a correspondingly large reduction in computing time. Consequently, once the problem geometry has been adopted, the four methods seem to be a self-contained tool for validation of the results. Due to the small number of unknowns, surprisingly complex problems can be solved on standard personal computers.

Although, of the four methods, some have advantages in solving specific problems, when solving other problems they may have deficiencies. Therefore, none of them can be proclaimed as the best. Still, numerical results indicated that, in most cases, the Galerkin method used for solving the two-potential equation with vector **D** as the unknown could, on average, be considered as the most accurate, stable, and reliable.

Finally, in the authors' opinion, this article demonstrates that the entire-domain approach extends greatly the applicability of the moment-method solutions when compared with the subdomain approach. Therefore, in spite of its relative mathematical and numerical complexity, it should not be considered a luxury. In our opinion, if we wish to promote the applicability of moment-method solutions to their extreme frontiers, the entire-domain approach is a necessity.

REFERENCES

1. Y. Nomura and T. Hatta, "The Theory of a Linear Antenna, I," Technical Report 17(1), Tohoku University, 1952.
2. R. F. Harrington, *Field Computation by Moment Methods*. Macmillan, New York, 1968.
3. A. Taflove, *Computational Electrodynamics: The Finite-Difference Time-Domain Method*. Artech House, Boston, MA, 1995.
4. B. D. Popović, *CAD of Wire Antennas and Related Radiating Structures*. Wiley, Chichester, 1991.
5. B. D. Popović and B. M. Kolundžija, "Analysis of Metallic Antennas and Scatterers," *IEE Electromagnetic Wave Series, No. 38*, London, 1994.
6. B. D. Popović and B. M. Notaroš, "Entire-Domain Polynomial Approximation of Volume Currents in the Analysis of Dielectric Scatterers, *IEE Proc. Microwave Ant. Propagat.*, Vol. 142, No. 3, June 1995, pp. 207–212.

7. B. M. Notaroš, "Numerical Analysis of Dielectric Bodies of Arbitrary Shape and Inhomogeneity in the Electromagnetic Filed" [in Serbian], DSc thesis, Department of Electrical Engineering, University of Belgrade, Belgrade, 1995.
8. T. K. Sarkar, E. Arvas, and S. Ponnapalli, "Electromagnetic Scattering from Dielectric Bodies," *IEEE Trans.*, Vol. AP-37, No. 5, May 1989, pp. 673–676.
9. C. C. Su, "Electromagnetic Scattering by a Dielectric Body with Arbitrary Inhomogeneity and Anisotropy," *IEEE Trans.*, Vol. AP-37, No. 3, March 1989, pp. 384–389.

BIOGRAPHIES

Branko D. Popović obtained his BSc, MSc, and DSc degrees from the University of Belgrade, Yugoslavia, in 1958, 1963, and 1967, respectively. He joined the EE Department of the University of Belgrade in 1959, where he was Teaching Assistant, Assistant Professor, Associate Professor and, since 1977, he has been Professor of Electrical Engineering.

He is the author or coauthor of 135 papers in professional journals and proceedings of conferences, the author of six university textbooks (one of which was published by Addison-Wesley in the U.S.), the principal author of the monograph *Analysis and Synthesis of Wire Antennas* (Research Studies Press, 1982), and the author of the monograph *CAD of Wire Antennas and Related Radiating Structures* (Wiley, 1991). He is the principal author of *Analysis of Metallic Antennas and Scatterers* (IEE, London), and is a fellow of the IEE (London). He is also the author or coauthor of over 40 projects dealing with problems in applied electromagnetics (mostly the design of antennas) and the author of a powerful general program, *WireZeus*, for the analysis and design of wire and related antennas.

He was awarded the Heinrich Hertz Premium of the British Institute of Electronic and Radio Engineers (1974), the James Clerk Maxwell Premium of the British Institution of Electrical Engineers (1985), and the Yugoslav Nikola Tesla Premium (1985), and a number of other Yugoslav awards.

He was elected a Corresponding Member of the Serbian Academy of Sciences and Arts in 1978, and a Member of the Academy in 1988.

Dr. Popović also served as Visiting Professor at Virginia Polytechnic Institute, Blacksburg, Virginia (1967–1969 and 1981–1982); with McGill University, Montreal, Canada (spring semester 1973); and with the Chengdu University, Chengdu, Sechuan, China (November–December 1984). He has given many lectures on his work in the U.S., Canada, England, The Netherlands, Denmark, Italy, and Turkey.

Branislav M. Notaroš was born in Zrenjanin, Yugoslavia, on January 2, 1965. He received BSc, MSc, and PhD degrees in electrical engineering from the Department of Electrical Engineering, University of Belgrade, Yugoslavia, in 1988, 1992, and 1995, respectively. He was awarded the Belgrade Trade Association Prize for the best MSc thesis in 1992. Since 1989 he has been a teaching assistant in electromagnetics, applied electromagnetics and fundamentals of electrical engineering, at the Department of Electrical Engineering, University of Belgrade. He is a coauthor of several articles, published in journals and presented at conferences. His research interests are in numerical analyses of metallic and/or dielectric antennas and scatterers.